Engineering and Applied Sciences
2022; 7(5): 63-70
http://www.sciencepublishinggroup.com/j/eas
doi: 10.11648/j.eas.20220705.12
ISSN: 2575-2022 (Print); ISSN: 2575-1468 (Online)

Evaluation on the Chloride Ion Penetration into Concrete Added Different Types of Admixture Using Industrial Byproducts

Nam Wook Kim

Department of Civil and Environmental Engineering, Honam University, Gwangju, Republic of Korea

Email address:
kimnw@honam.ac.kr

To cite this article:
Nam Wook Kim. Evaluation on the Chloride Ion Penetration into Concrete Added Different Types of Admixture Using Industrial Byproducts. *Engineering and Applied Sciences*. Vol. 7, No. 5, 2022, pp. 63-70. doi: 10.11648/j.eas.20220705.12

Received: August 21, 2022; **Accepted**: September 13, 2022; **Published**: September 28, 2022

Abstract: In recent years, chloride ion stagnation has been reported in concrete with high chloride ion penetration resistance, even if the material age increases, the depth of chloride ion penetration does not change. It has been confirmed that most of the collected cores are not only at the chloride ion stop position, but also at the surface layer, and that this long-term chloride ion stagnation phenomenon has not been reported, which is a very valuable case. In order to properly predict chloride ion penetration, it is necessary to grasp and consider the above stagnation phenomenon. Therefore, the purpose of this study is to discuss the presumption of chloride ion penetration considering the stagnation of chloride ion penetration. In this study, the presumption of chloride ion penetration was studied considering chloride ion stagnation. The findings obtained in this study are shown below. In the case of low water bonding material ratio, chloride ion penetration is likely to stagnate in all test specimens of ordinary concrete, fly ash concrete and blast furnace slag concrete studied in this study. Based on the liquid water infiltration position determined by visual observation, a chloride ion infiltration presumption model was prepared for each cement species considering the effect of advection. In dense concrete structures with stagnant chloride ion penetration, it is confirmed that Fick's diffusion equation currently prescribed in the presentation. For blast furnace slag concrete with many coarse gaps and no chloride ion penetration stagnation, it is shown that it can be handled by using the chloride ion penetration estimation model of ordinary concrete.

Keywords: Chloride Ion Penetration, Admixtures, Industrial Byproduct, Fick’s Diffusion Law, Durability

1. Introduction

In the durability inspection design of concrete chloride ion damage, Fick's diffusion law is used to predict chloride ion penetration by presuming surface chloride ion concentration C_0 and apparent diffusion coefficient D_a. However, it has been pointed out that C_0 increases and D_a decreases as the age of the material increases. Therefore, the present method of predicting chloride ion penetration may be too safe.

In recent years, chloride ion stagnation has been reported in concrete with high chloride ion penetration resistance, even if the material age increases, the depth of chloride ion penetration does not change. [1-3]

It has been confirmed that most of the collected cores are not only at the chloride ion stop position, but also at the surface layer, and that this long-term chloride ion stagnation phenomenon has not been reported, which is a very valuable case. In order to properly predict chloride ion penetration, it is necessary to grasp and consider the above stagnation phenomenon.

Therefore, the purpose of this study is to discuss the presumption of chloride ion penetration considering the stagnation of chloride ion penetration.

2. The Governing Equation for Chloride Ion Penetration Behavior

The physical movement of chloride ion into concrete is expressed by diffusion and advection. Therefore, in this study,

chloride ion penetration is deduced using the advection diffusion equation of the following formula. [4-6]

$$\frac{\partial C}{\partial t} = D_{av}\frac{\partial^2 C}{\partial x^2} - V\frac{\partial C}{\partial x} \quad (1)$$

Here, C is the total chloride ion content (kg/m^3), t is the time (year), x is the distance (cm), D_{av} is the average diffusion coefficient, and V is the average velocity (cm/s).

In Formula (1), the solution to the chloride ion penetration estimation formula under the condition that the porous medium is semi-infinite column is shown in Formula (2).

$$\frac{C(x,t)}{C_0} = 0.5\left[\begin{matrix} erfc\frac{x-V_t}{2\sqrt{D_{av}t}} \\ +exp\left(\frac{V_x}{D_{av}}\right)erfc\left(\frac{x+V_t}{2\sqrt{D_{av}t}}\right)\end{matrix}\right] \quad (2)$$

Here, *efrc* is a complementary error function and *exp* is an exponential function.

In addition, in this study, the mean diffusion coefficient over a certain period of time is set to the mean diffusion coefficient D_{av}, which is calculated by equation (3).

$$D_{av} = \frac{\sum_{t=1}^{T} D_t \times t}{\sum_{t=1}^{T} t} \quad (3)$$

Here, D_t is the diffusion coefficient at any point in time t and T is the total life span.

The average velocity V of advection is calculated from the porosity and permeability of equation (4).

$$V = \frac{\kappa}{\varphi}\frac{\partial h}{\partial x} \quad (4)$$

Here, $\frac{\partial h}{\partial x}$ is the dynamic water gradient (MPa/m), κ is the permeability (m/s), and φ is the porosity of the material, and in this study $\frac{\partial h}{\partial x}$ is the constant of 0.1 (MPa/m).

The porosity required to calculate the average velocity V of advection is calculated from the water absorption measured experimentally and the infiltration depth of liquid water.

$$\varphi = \frac{1000 \times M}{Wf} \quad (5)$$

Here, M is the water absorption (gm/mm^2) and Wf is the limit position (cm) of liquid water infiltration.

The correlation between water permeability and pore radius has been reported. In this study, equation (6) is used to calculate the radius of pore represented.

$$\kappa = 2.51 \times 106 \times 10^6 \times r^{3.35} \quad (6)$$

Here, r is the representative pore radius (m).

The radius of the representative pore is calculated by equation (7) based on Washburn's law based on the relationship between liquid water immersion and capillary force.

$$\mathrm{r(m)} = \sqrt{\frac{4\mu}{P_0}} \times \frac{Wf}{\sqrt{t}} \quad (7)$$

Here, t is the time (seconds), 4μ is the viscosity (pa-s), and P_0 is the pressure (pa). In this study, μ is the constant of 0.0012 (pa-s) and P_0 is the constant of 10,1300 (pa).

The surface chloride ion concentration C_0 increases with time and converges at a certain value.

$$C_0(t) = C_0(1 - exp^{-\alpha t}) \quad (8)$$

Here, α is the environmental factor, t is the time (year) and C_0 is the maximum surface chloride ion concentration (kg/m^3), and in this study, α is a constant of 0.45.

3. Determine the Parameters Required for Analysis

3.1. Overview of Chloride Ion Water Immersion Test

To clarify the effect of concrete combination and environmental conditions on chloride ion permeability and the relationship between liquid water infiltration area and salt permeation stop position. In addition, chloride ion water immersion test was carried out to obtain parameters used in chloride ion penetration estimation formula. [7-10]

In order to eliminate the effects of hydration reaction and study chloride ion permeability, concrete specimens with Φ100×200mm size were used more than a year after production. The factors and experimental levels of the specimens were shown in Tables 1 and 2.

The concentration of chloride ion water used in immersion was set to 10% and cracked in 3 months and 6 months, and the depth of liquid water infiltration was determined visually and the amount of chloride ion was determined by titration. In addition, the measurement method of weight gain due to liquid water infiltration is described below.

Table 1. *Used factors and conditions of research.*

Contents	Kinds	Remarks
Cement and admixtures	Cement: Ordinary Portland cement (PC) Admixtures: Fly ash (FA) Blast furnace slag (BS)	
Water-Cement ratio (%)	40, 55, 70	
Direction of deposition	Horizontal direction Vertical top opening Vertical top coating	
Conditions of deposition	Drying and moisture condition (repetition of 1 day salt immersion, 6 days drying oven)	

Table 2. *Mixing design of used specimen.*

Kinds	W/C (%)	Unit weight (kg/m^3)				
		W	C	B	S	G
PC	40	180	551	-	709	979
PC	55	180	328	-	805	986
PC	70	180	258	-	886	961
FA	40	173	356	86	695	999
FA	55	173	251	63	792	1008
FA	70	173	198	59	874	986
BS	40	176	219	219	696	1001
BS	55	176	159	159	792	1009
BS	70	176	126	126	874	986

3.1.1. Weighting

In order to compare the relationship between the water absorption of the specimen and the position of liquid water infiltration, weight measurement was carried out regularly once a week to grasp the timing of liquid water infiltration. In order to evaluate the weight by water absorption per unit area, image analysis software is used to calculate the surface area.

3.1.2. Determination of Liquid Water Infiltration Position

Referring to the Liquid Water Infiltration Location Test conducted by Islam et al., the location of liquid water infiltration was determined. [11, 12]

It has been pointed out that the liquid water infiltration area corresponds to the chloride ion penetration stop position, and the relationship with the chloride ion penetration stop position is confirmed by grasping the limit position of liquid water infiltration. A compressive strength tester was used to crack the specimen after a certain period of chloride ion water immersion. About 10 locations of liquid water infiltration were determined using caliper. [13, 14]

3.1.3. Potential Differential Titration

In order to grasp the salt permeability, the total chloride ion content was determined by potential differential titration test according to NT Build 492. [15, 16]

3.2. Results of Chloride Ion Water Immersion Test

3.2.1. Weighting Results

The water absorption M per unit area was obtained from the weight measurement results of 6 months of age. The relationship between water binding material ratio and water absorption is shown in Figure 1.

From the Figure, it can be confirmed that the water absorption M increases with the ratio of water bonding materials, and that the inclination varies depending on the presence or absence of mixing materials. Therefore, the regression formula for the ratio of water absorption M to water binding material is calculated for each mixture. This formula is shown in equations (9), (10) and (11).

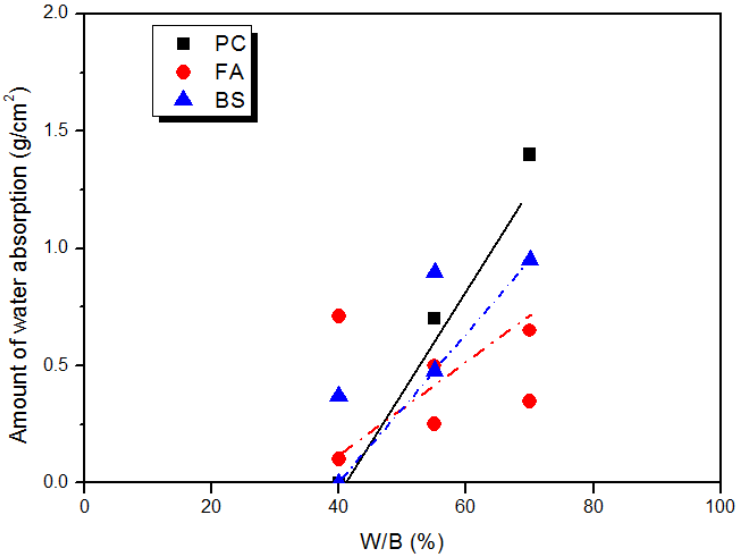

Figure 1. *Relationship between water-binder ratio and water absorption.*

$$\text{PC: } M = 0.0365 \times {}^{W}/_{B} - 1.57 \quad (9)$$

$$\text{FA: } M = 0.0127 \times {}^{W}/_{B} - 0.236 \quad (10)$$

$$\text{BS: } M = 0.0279 \times {}^{W}/_{B} - 1.15 \quad (11)$$

3.2.2. Results of Liquid Water Infiltration Position Measurement

The average value of liquid water infiltration limit position Wf was calculated from the results of 6 months of material age measurement. The relationship between the ratio of water

binder and the average liquid water infiltration limit position is shown in Figure 2.

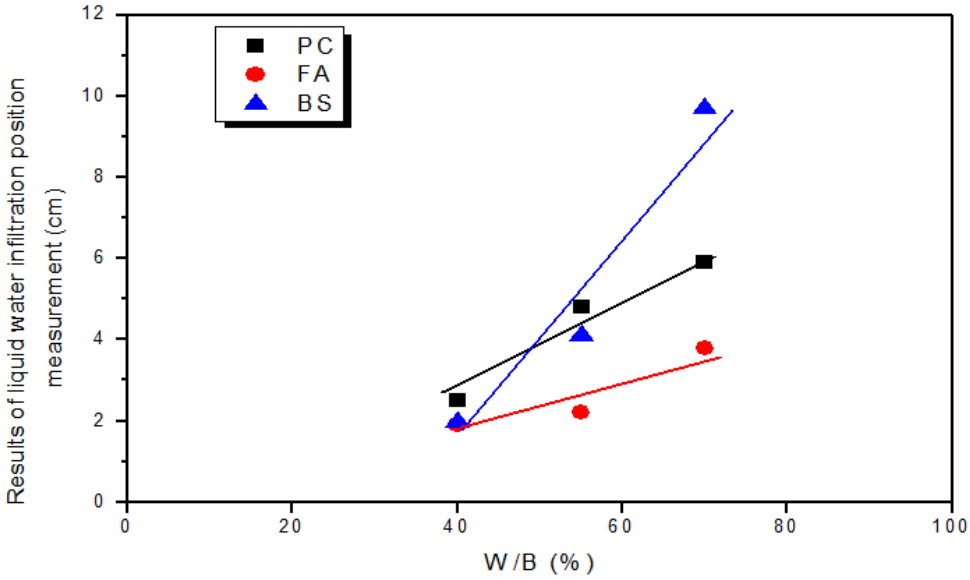

Figure 2. *Relationship between water-binder ratio and average liquid water infiltration limit position.*

From Figure 2, it can be confirmed that the average liquid water infiltration limit position increases with the water binding material ratio as well as the water absorption *M*, and that the inclination varies depending on the presence or absence of the mixture. Therefore, with respect to the average liquid water infiltration limit position *Wf*, the regression formula with the ratio of water-binder is calculated for each cement type. This formula is shown in Equations (12), (13), (14).

$$\text{PC: } Wf = 0.123 \times {}^{W}/_{B} - 1.67 \quad (12)$$

$$\text{FA: } Wf = 0.0653 \times {}^{W}/_{B} - 1.22 \quad (13)$$

$$\text{BS: } Wf = 0.121 \times {}^{W}/_{B} - 9.14 \quad (14)$$

3.2.3. Consideration of Variations in Liquid Water Infiltration Locations

Since the liquid water chloride ion penetration stop position is controlled by the liquid water infiltration limit position *Wf*, it is necessary to calculate *Wf* to properly predict chloride ion penetration behavior.

The fracture surface of the specimen after cracking is shown in Figure 3. From the Figure 3, it can be confirmed that the infiltration surface of liquid water is not straight, but uneven. In addition, Figure 3 shows the relationship between the ratio of water binder and the standard deviation *Sd* of liquid water infiltration position.

From Figure 4 and Figure 5, it can be seen that not only the absolute value of *Wf* but also *Sd* is small, but also *Wf* and *Sd* are large for concrete with high water bonding ratio.

Figure 5 shows the relationship between *Wf* and *Sd*, but it can be confirmed that there is a linear correlation.

Therefore, in this study, *Sd* is calculated from *Wf* using regression equations (15), (16) and (17).

$$\text{PC: } Sd = 0.169 \times Wf \quad (15)$$

$$\text{FA: } Sd = 0.223 \times Wf \quad (16)$$

$$\text{BS: } Sd = 0.368 \times Wf \quad (17)$$

Figure 3. *Broken section of the test specimen.*

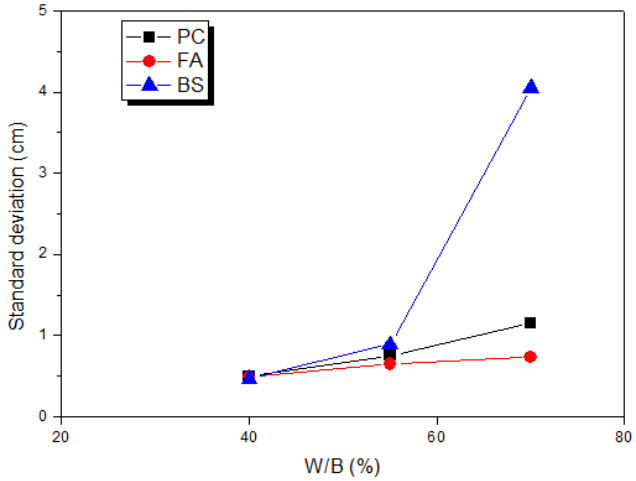

Figure 4. *Relationship between water-binder ratio and variation.*

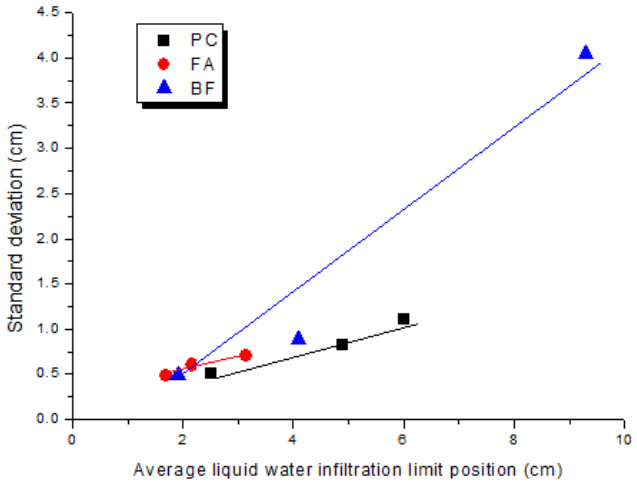

Figure 5. *Relationship between average liquid water infiltration limit position and standard deviation.*

3.2.4. Potential Difference Titration Results

The total chloride ion content was determined according to depth by potential differential titration test at the age of 3~6 months. In any cement species, the results of chloride ion stagnation were shown in Figure 6~Figure 8 for each cement species.

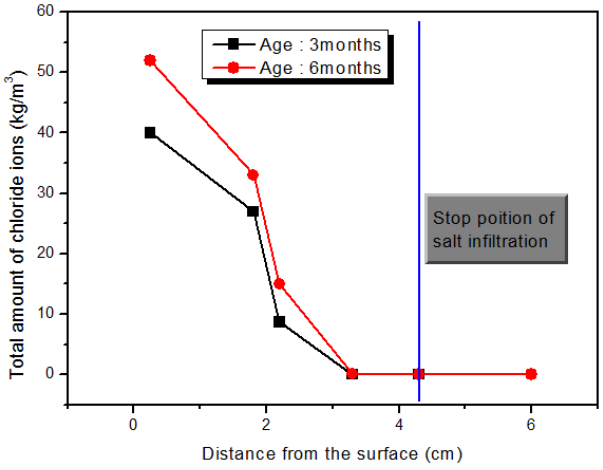

Figure 6. *Total amount of chloride ions (PC).*

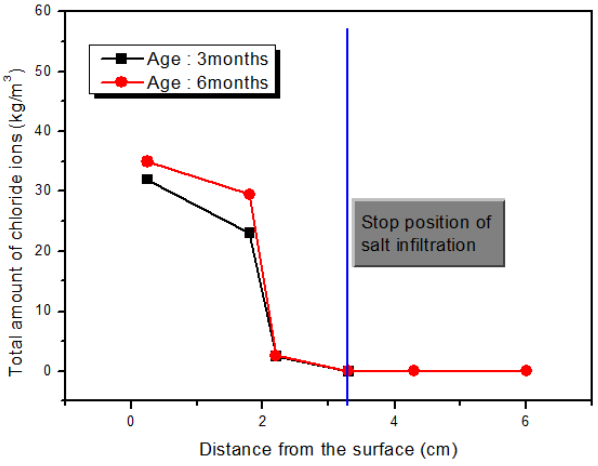

Figure 7. *Total amount of chloride ions (FA).*

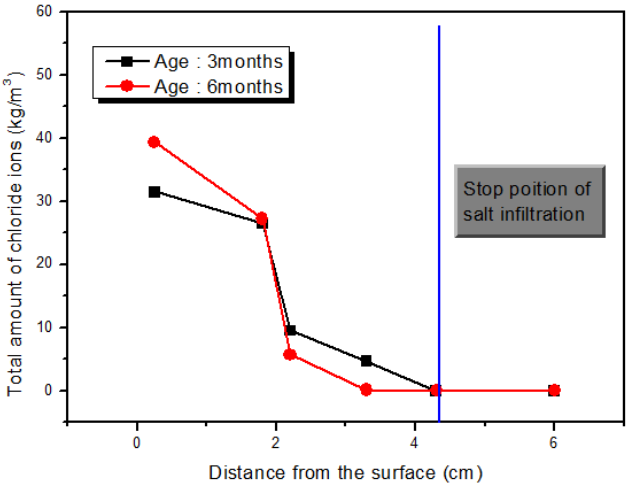

Figure 8. *Total amount of chloride ions (BF).*

According to Figure 6~Figure 8, although there is a difference in immersion period between three months and six months of material age, chloride ion penetration is considered to be stagnant because chloride ion penetration is hardly observed during that period. Previous studies have reported chloride ion penetration stagnation in concrete using admixture, but it has been shown that chloride ion penetration can stagnate in concrete with low water-bonding ratio.

Although no abnormalities were found in the test specimens shown in Figures 6~8, some of the test specimens were infiltrated from outside the infiltration surface due to the use of deteriorated epoxy resins in coatings to prevent liquid water from entering outside the infiltration surface.

The cleavage surface is shown in Figure 9. Therefore, it is judged that it is inappropriate to calculate the diffusion coefficient based on the results of this measurement, and that Dav, which was obtained for each cement species in the past by Islam et al., is shown in Forms (18), (19), (20).

Figure 9. *Fraction surface of the test specimen.*

$$\text{PC: } D_{av} = 0.646 \times {}^{W}/_{B} - 24.7 \quad (18)$$

$$\text{FA: } D_{av} = 0.119 \times {}^{W}/_{B} - 4.53 \quad (19)$$

$$\text{BF: } D_{av} = 0.042 \times {}^{W}/_{B} - 1.14 \quad (20)$$

Based on Formula (9)~(20), the parameters required in the formula shown in the previous chapter are calculated from the conditions of the combination. Accordingly, a framework for inferring chloride ion permeability at any age based on the conditions of mixing is constructed.

4. Verification of Chloride Ion Penetration Estimation Model

Core specimens were collected from the actual structural part of the material age and chloride ion content was determined. The validity of the model is verified by comparing the measured values with those calculated from the chloride ion penetration estimation model constructed in the previous chapter.

4.1. Core Extraction from Actual Structures and Salt Distribution Determination

A total of 12 cores (φ100×200mm) of adjacent blast furnace slag concrete and fly ash concrete were collected in 2010, about 10 years after completion.

BF is a revetment structure on the left side of the blast furnace cement B, less than 50% of the water bond material, FA is a revetment structure on the right side of the photograph with 30% internal replacement and 45% water bond material. In addition, the fourth tier, which is the lowest tier of the sea, is covered with oysters on the surface, the third tier of the sea is located above the high tide, and the land is located in the atmosphere of the sea without splashing waves. [17, 18]

4.1.1. Potential Differential Titration Test

The salt distribution was determined by using the surface layer 100mm of the core.

4.1.2. Chloride Ion Penetration Estimation

The parameters obtained so far were used to estimate chloride ion penetration and compared with the actual chloride ion distribution. The water binding material ratio of blast furnace slag concrete was set to 50%.

4.2. Results of Core Measurement from Actual Structures

The salt distribution of each cement species is shown in Figures 10 and 11. From Figure 10 and Figure 11, it is confirmed that the chloride ion penetration stop position of each cement species is approximately the same, and that fly ash concrete has higher chloride ion resistance than blast furnace slag concrete. This suggests that the combination has a significant effect on chloride ion penetration resistance.

Although the combination is the same, the difference in total chloride ion content can be attributed to the difference in chloride ion supply due to the difference in core extraction height. In this result, the total chloride ion content of the land-side core in the sea atmosphere was smaller than that of the sea-side.

In addition, although this difference can be seen on the surface, the chloride ion penetration stop position is the same for each combination, so it can be thought that chloride ion stagnation is occurring. The parameters obtained so far were used in the chloride ion penetration formula to infer chloride ion penetration and compare it with the actual salt distribution. For comparison with the measured value, the concentration of chloride ions on the surface is the same as the measured value.

In addition, comparisons based on Fick's diffusion equation are also discussed. The actual measured values, estimation values based on the proposed model, and calculation values based on Fick's diffusion equation are shown in Figures 12 and 13.

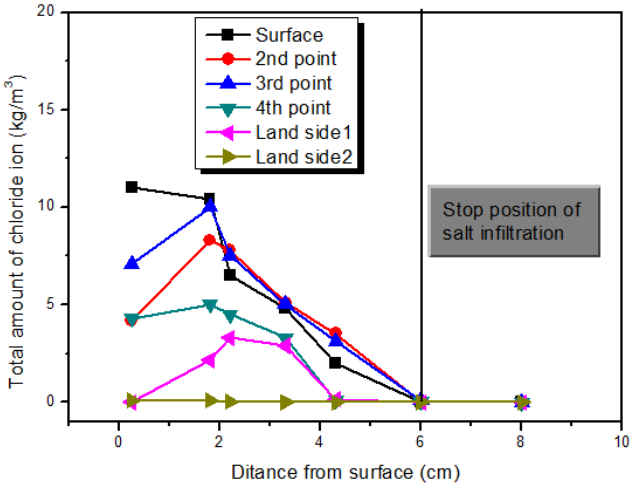

Figure 10. *Chloride distribution of BB at the time of extraction.*

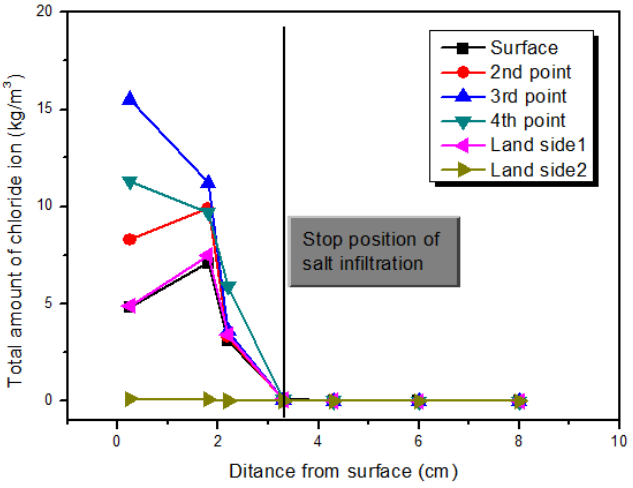

Figure 11. *Chloride distribution of FA at the time of extraction.*

The presumption results of fly ash concrete are shown in Figure 12. Based on the model proposed in this study, it can be confirmed that the chloride ion content close to the measured value is estimated.

On the other hand, the value obtained from Fick's diffusion equation (hereinafter referred to as Fick's value) is significantly higher than the measured value. Since the difference between the measured value and the Fick value

increases with age of the material, it is considered that the durability design based on the Fick value is not economical in concrete structures with high chloride ion penetration resistance and long service years.

Next, the results of blast furnace slag concrete are shown in Figure 13. Compared with the estimates of the proposed model, the Fick value is closer to the actual measured value.

In addition, the model's estimates are compared with the actual measurements to represent the dangerous side.

Therefore, after the next section, the model of core extraction from other structures is verified and the chloride ion penetration estimation model of blast furnace slag concrete is corrected.

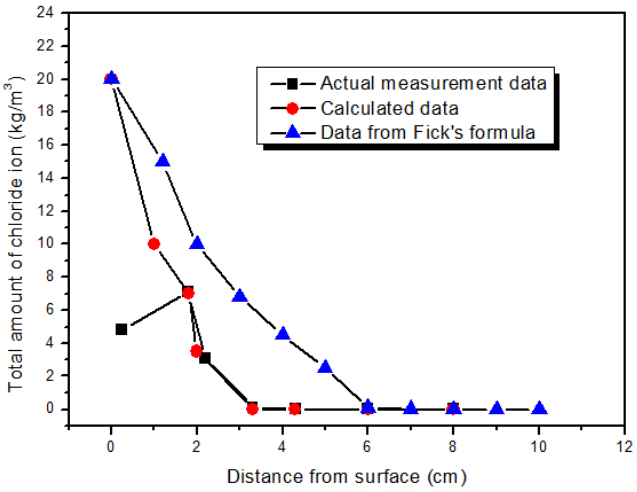

Figure 12. *Estimation results of FA (at the Top point).*

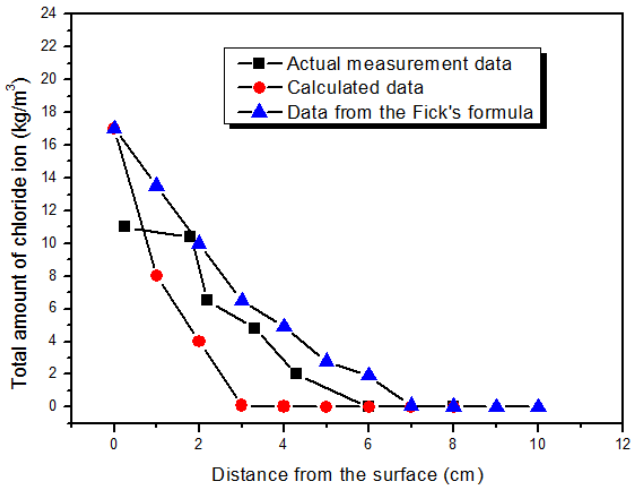

Figure 13. *Estimation results of BF (at the Top point).*

5. Conclusion

In this study, the presumption of chloride ion penetration was studied considering chloride ion stagnation.

The findings obtained in this study are shown below.

(1) In the case of low water bonding material ratio, chloride ion penetration is likely to stagnate in all test specimens of ordinary concrete, fly ash concrete and blast furnace slag concrete studied in this study.

(2) Based on the liquid water infiltration position determined by visual observation, a chloride ion infiltration presumption model was prepared for each cement species considering the effect of advection.

(3) In dense concrete structures with stagnant chloride ion penetration, it is confirmed that Fick's diffusion equation currently prescribed in the presentation.

(4) For blast furnace slag concrete with many coarse gaps and no chloride ion penetration stagnation, it is shown that it can be handled by using the chloride ion penetration estimation model of ordinary concrete.

Acknowledgements

This work was grant funded by the Ministry of SMEs and Startups of the Korea government (No. S3290334).

References

[1] American Concrete Institute (2011), "Building Code Requirements for Structural Concrete and Commentary", ACI 318-11.

[2] Bentz, E. C., (2003), "Probabilistic Modeling of Service Life for Structures subjected to Chloride", ACI Materials Journal, 72 (5), 391-397.

[3] Ishida, T et al., (2018), "Numerical Simulation of Early age Cracking of Reinforced Concrete Bridge Decks with a Full-3D Multiscale and Multi chemo-physical Integrated analysis" Applied Science, 8 (394), 56-63.

[4] Kinomura, K et al., (2019), "Extensive Modeling of Peculiar Hydration in Fine Micro-Pore Structures Applicable to Integrated Thermodynamic Analysis for Portland Cement", Applied Science, 9 (2137), 86-94.

[5] Na, U. J et al., (2012), "Stochastic Model for Service Life Prediction of RC Structures Exposed to Carbonation using Random Field Simulation", Journal of KSCE, 16 (1), 133-143.

[6] Suryanto, B et al., (2012), "An Investigation into the Long-term Excessive Deflection PC Viaducts by using 3D Multi-scale Integrated Analysis", Journal of Advanced Concrete Technology, 10 (2), 47-58.

[7] Stewart, M. G et al., (2007), "Spatial time-depentent Relaibility Analysis of Corrosion Damage and the Timing of First Repair of RC Structures", Engineering Structures, 38 (5), 1457-1464.

[8] Tang, L., (2008), "Engineering Expression of the Clinconc Model for Prediction of Free and Total Chloride Ingess in Submerged Marine Concrete", Cement and Concrete Research, 38 (4), 1092-1097.

[9] Thomas, M., (1996), "Chloride Thresholds in Marine Concrete", Cement and Concrete Research, 24 (4), 513-519.

[10] Arya, C et al., (1990), "An Assessment of Four Methods of Determining the Free Chloride Contents of Concrete", Materials Structures, 23 (2), 319-330.

[11] Islam, MD. S et al., (2008), "Simulation of Chloride ion Profile into Repaired Crack Concrete", Journal of Civil Engineering, 36 (1), 23-42.

[12] Abdullah, AL. M., (2017), "Experimental Investigation of Chloride Ion Penetration and Reinforcement Corrosion in Reinforced Concrete Member", 7 (1), 26-29.

[13] Berke, N. S et al., (1994), "Predicting Chloride Profiles in Concrete", Corrosive Engineering, 1 (2), 234-239.

[14] Saraswathy, V et al., (2007), "Evaluation of Corrosion Resistance of Portland Pozzolana Cement and Fly ash blended Cements in Pre-cracked Reinforced Concrete Slabs under Accelerated Testing Conditions", Materials Chemistry Physics, 104 (2-3), 356-361.

[15] NT Build 492. "Chloride Migration Coefficient from Non-Steady State Migration Experiments".

[16] ASTM C 1202, "Standard Test Method for Electrical Indication of Concrete's Ability to Resist Chloride Ion Penetration".

[17] Song, H. W et al., (2006), "Analysis of Corrosion Resistance of Inhibitors in Concrete using Electrochemical Studies", Met and Mat Int., 12 (4), 232-329.

[18] Ann, K. Y et al., (2007), "Chloride Threshold Level for Corrosion of Steel in Concrete", Corrosive Science, 49 (3), 4113-4123.